The effect of the quasi-biennial oscillation on the Madden-Julian oscillation in the Met Office Unified Model Global Ocean Mixed Layer configuration

Received: 29 September 2017 | Revised: 12 December 2017 | Accepted: 24 February 2018

DOI: 10.1002/asl.816

Atmospheric Science Letters RMetS

RESEARCH ARTICLE

The effect of the quasi-biennial oscillation on the Madden–Julian oscillation in the Met Office Unified Model Global Ocean Mixed Layer configuration

Joshua C. K. Lee[1] | Nicholas P. Klingaman[2]

[1]Department of Meteorology, University of Reading, Reading, UK

[2]National Centre for Atmospheric Science-Climate, University of Reading, Reading, UK

Correspondence
N. P. Klingaman, Department of Meteorology, University of Reading, Reading, Berkshire RG6 6BB, UK.
Email: nicholas.klingaman@ncas.ac.uk

Funding information
Natural Environment Research Council, Grant/Award number: NE/L010976/1

Using multi-decadal simulations, we investigate the relationship between the quasi-biennial oscillation (QBO) and the Madden–Julian oscillation (MJO) in the Global Ocean Mixed Layer configuration of the Met Office Unified Model (MetUM-GOML1) at two horizontal resolutions (approximately 200 and 90 km at the equator). MetUM-GOML1 produces a weak and insignificant correlation between QBO winds and mean MJO amplitude in boreal winter, in contrast to the significant anti-correlation in reanalysis. While reanalysis shows the easterly QBO favors stronger Maritime Continent MJO activity, MetUM-GOML1 displays stronger West Pacific MJO activity. The biased QBO–MJO relationship in MetUM-GOML1 may be due to weak QBO-induced temperature anomalies in the tropical tropopause layer, or to errors in MJO vertical structure.

KEYWORDS
climate, convection, general circulation model experiments, stratosphere, teleconnections, Tropics

1 | INTRODUCTION

The Madden–Julian oscillation (MJO) (Madden & Julian, 1971) is a major component of tropical tropospheric intraseasonal variability (≈30–70-day period), characterized by coherent regions of deep convection, enhanced rainfall and associated zonally overturning circulations. Events propagate east at ≈5 m/s, often starting in the equatorial Indian Ocean and moving through the Maritime Continent to the Pacific (Zhang, 2005). Suppressed convection occurs east and west of the active phase, resulting in a zonal wavenumber-1 pattern.

Although the past decade has seen improvements in understanding and predicting the MJO, general circulation models (GCMs) often fail to represent essential MJO features (e.g., Jiang et al., 2015). This is often attributed to a poor understanding of key MJO physics (e.g., Liu et al., 2016; Zhang, 2005). Various changes to model physics and ensemble-generation methods have improved MJO prediction skill (e.g., Hudson, Marshall, Yin, Alves, & Hendon, 2013; Kang, Jang, & Almazroui, 2014; Wu et al., 2016). In the Met Office Unified Model (MetUM), Shelly et al. (2014) found that coupling the atmosphere to a dynamical ocean advanced useful MJO skill by 3–5 days. Klingaman and Woolnough (2014a) demonstrated that increasing the sensitivity of convection to tropospheric moisture, via higher mixing entrainment and detrainment rates, improved skill for a limited set of cases, as well as the simulated MJO in the MetUM climate model.

Recent studies suggest that the stratospheric quasi-biennial oscillation (QBO) (Baldwin et al., 2001) may modulate MJO strength and predictability (e.g., Marshall, Hendon, Son, & Lim, 2017; Son, Lim, Yoo, Hendon, & Kim, 2017; Yoo & Son, 2016). The QBO comprises a quasi-periodic (≈28 months) reversal of equatorial 10–100-hPa zonal winds (Baldwin et al., 2001). The reversal propagates slowly downwards at ≈1 km/month to the tropopause, before the next phase descends. The QBO influences

tropical upper-tropospheric temperature and winds and thus may affect the large-scale environment for the MJO (e.g., Garfinkel & Hartmann, 2011; Giorgetta, Bengtsson, & Arpe, 1999; Huang, Hu, Kinter, Wu, & Kumar, 2012). In particular, easterly QBO (EQBO) phases are associated with a colder and higher-altitude tropical tropopause layer (TTL), which reduces static stability relative to westerly QBO (WQBO) phases (e.g., Fueglistaler et al., 2009; Nishimoto & Yoden, 2017). On seasonal scales, the colder TTL may strengthen and deepen equatorial convection during EQBO (Collimore, Martin, Hitchman, Huesmann, & Waliser, 2003; Nie & Sobel, 2015). GCMs may be useful tools to explore stratosphere–troposphere coupling mechanisms (e.g., Yoden, Bui, & Nishimoto, 2014); however, many GCMs fail to generate a QBO due to coarse stratospheric vertical resolution (e.g., Charlton-Perez et al., 2012).

Yoo and Son (2016) demonstrated that the boreal-winter MJO is typically stronger during EQBO than WQBO, using 36 years of reanalysis winds and MJO data. Enhanced MJO amplitude in EQBO is particularly evident near the Maritime Continent (Son et al., 2017). Marshall et al. (2017) found higher MJO skill during EQBO winters, using sub-seasonal re-forecasts with the Predictive Ocean Atmosphere Model for Australia. In this emerging area of research, no study has investigated whether a climate model can reproduce this relationship, possibly because many GCMs struggle to internally generate the QBO or the MJO, or both. Here, we use the MetUM Global Ocean Mixed Layer coupled configuration (MetUM-GOML1) (Hirons, Klingaman, & Woolnough, 2015), which is one of a small handful of GCMs to simulate the QBO and MJO well (section 3.1) (Figure 1). MetUM-GOML1 also lacks an El Niño–Southern Oscillation (ENSO), due to its one-dimensional ocean, which is advantageous as ENSO may conflate the QBO–MJO relationship (Yoo & Son, 2016). Section 2 contains more details on MetUM-GOML1 and our methods. We investigate the QBO–MJO relationship in MetUM-GOML at two horizontal resolutions (section 3) and discuss and summarize our conclusions (section 4).

2 | MODEL, DATA AND METHODS

2.1 | MetUM-GOML1 configuration

MetUM-GOML1 comprises MetUM Global Atmosphere 3.0 (GA3) (Walters et al., 2011) coupled every 3 hr to the multi-column *K* profile parameterization (MC-KPP) mixed-layer ocean. To correct for the lack of ocean dynamics in MC-KPP and for biases in GA3 surface fluxes, prescribed increments to ocean temperature and salinity are applied to constrain the ocean towards a target mean state. These increments vary horizontally, vertically and with the seasonal cycle (Hirons et al., 2015). Here, the increments constrain the ocean mean state to the 1980–2009 climatology from Smith and Murphey (2007). Because the increments are a prescribed repeating seasonal cycle, not a relaxation, they do not damp variability. We use the "near-global" coupling domain from Hirons et al. (2015), in which GA3 and MC-KPP are coupled at all ocean gridpoints that are never covered by sea ice, which is prescribed as the 1980–2009 mean seasonal cycle from the Hurrell, Hack, Shea, Caron, and Rosinski (2008) data set. At all uncoupled points, SST is prescribed from the 1980–2009 mean seasonal cycle of Smith and Murphey (2007).

The GOML1 configuration here differs from Hirons et al. (2015); here, the GA3 rates of mixing entrainment and detrainment for deep and mid-level convection are increased by 50%. Klingaman and Woolnough (2014b) showed that this produced a stronger MJO with more coherent propagation, particularly when GA3 was coupled to MC-KPP, although Bush, Turner, Woolnough, Martin, and Klingaman (2015) found these sub-seasonal improvements were associated with degradations to the tropical mean state, particularly in West Pacific precipitation.

We use GOML1 at two horizontal resolutions: 1.875° longitude × 1.25° latitude (hereafter "GOML1-LR") and 0.83 × 0.55° (hereafter "GOML1-HR"). Both have 85 points in the vertical and a model lid at 85 km. "High-top" GCMs with finer stratospheric vertical resolution, including MetUM, have improved representations of the mean state and variability of the stratosphere, including the QBO (e.g., Charlton-Perez et al., 2012; Hardiman, Butchart, Hinton, Osprey, & Gray, 2012; Osprey, Grey, Hardiman, Butchart, & Hinton, 2013).

For GOML1-LR, we perform a three-member ensemble of 25-year simulations (75 years total). For GOML1-HR, we perform a single 59-year simulation. We analyse boreal winter (December–February [DJF]) only, as the observed MJO–QBO relationship is strongest then (Yoo & Son, 2016). There are 72 (58) DJF seasons in GOML1-LR (GOML1-HR).

2.2 | Data sets and indices

Winds and temperatures for 1979–2014 are obtained from the European Centre for Medium-range Weather Forecasts (ECMWF) Interim reanalysis (ERA-Interim) (Dee et al., 2011). The QBO phase is computed from the equatorial (0°N) zonal-mean zonal wind at 50 hPa ($\overline{U}_{50}$). WQBO is defined when $\overline{U}_{50} > 5$ m/s; EQBO is defined when $\overline{U}_{50} < -5$ m/s.

MJO strength and phase are determined by daily 1979–2014 real-time multivariate MJO (RMM) indices, RMM1 and RMM2 (Wheeler & Hendon, 2004), computed from National Oceanic and Atmospheric Administration satellite-derived outgoing long-wave radiation (OLR) and National Centers for Environmental Prediction reanalysis zonal winds at 850 and 200 hPa. RMM1 represents MJO variability in the Maritime Continent; RMM2 represents the anti-correlation of convective activity between the Indian

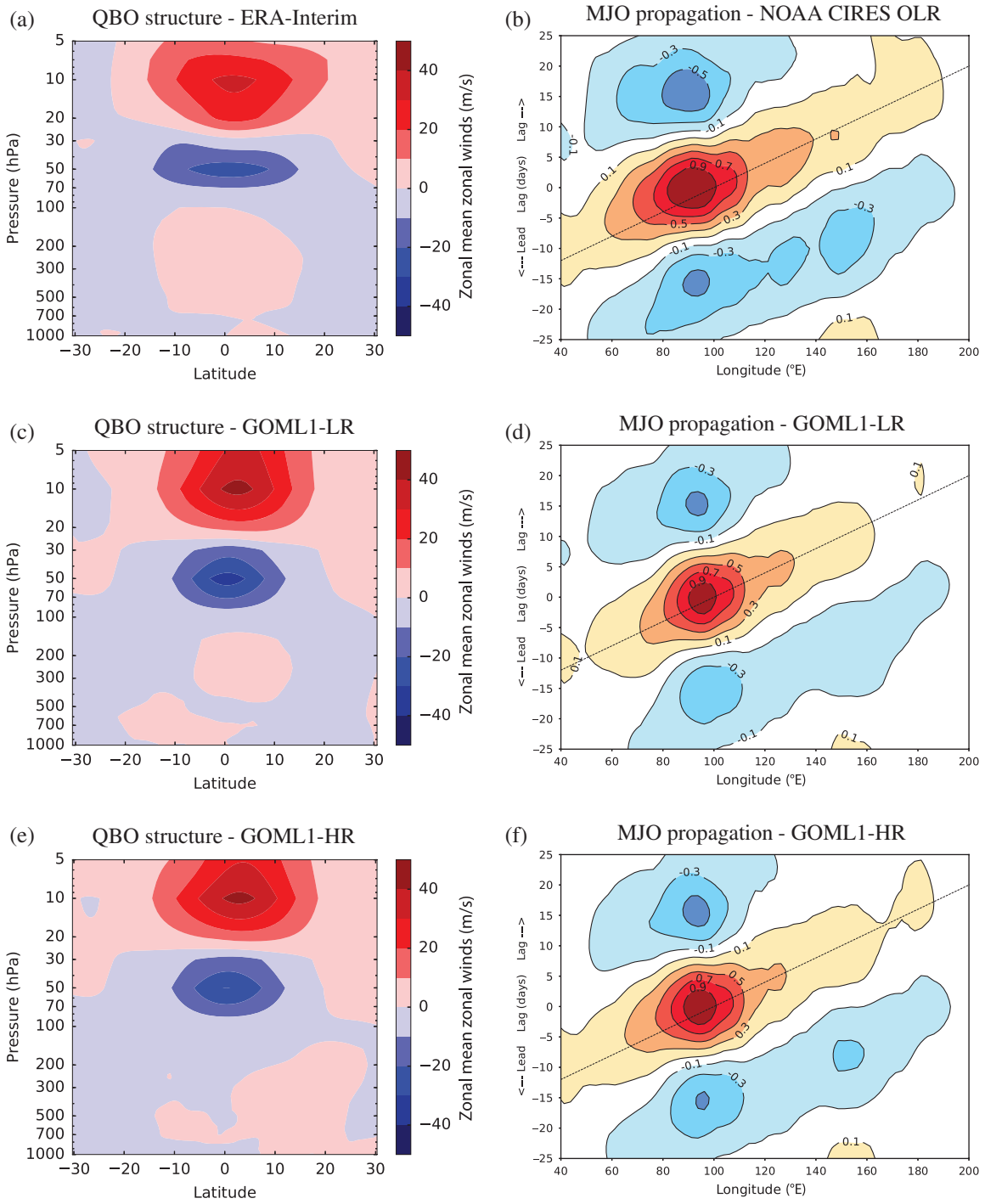

FIGURE 1 Panels (a), (c) and (e) show differences in zonal-mean zonal wind for EQBO minus WQBO composites as a diagnostic of QBO structure. Panels (b), (d) and (f) show regressions of latitude-averaged (10°S–10°N), bandpass-filtered (20–80 days) OLR, against itself at 100°E, as a diagnostic of MJO propagation; dotted lines show a phase speed of 5 m/s. Data from (a) ERA-Interim reanalysis (1979–2014), (b) National Oceanic and Atmospheric Administration satellite-derived OLR (1989–2008), (c, d) MetUM-GOML1 low-resolution simulations and (e, f) MetUM-GOML1 high-resolution simulations. See section 2 for details of model simulations, data sets and QBO compositing method

and West Pacific Oceans. The daily MJO amplitude is $\sqrt{\mathrm{RMM1}^2+\mathrm{RMM2}^2}$. Amplitudes ≥1 are considered "MJO active days." The RMM1 and RMM2 phase space is divided into eight phases, as in Wheeler and Hendon (2004). For simplicity, we refer to the combination of Wheeler and Hendon (2004) RMM indices and ERA-Interim $\overline{U}_{50}$ as "reanalysis."

For reanalysis, any ENSO influence is removed by excluding strong ENSO periods, following Yoo and Son (2016). A 3-month running-mean of Niño3.4 SST anomalies (average of 170°–120°W, 5°N–5°S) is computed from the Hadley Centre data set (Rayner et al., 2003) for 1979–2014. Strong ENSO periods are those with anomalies larger than ±1.0°C.

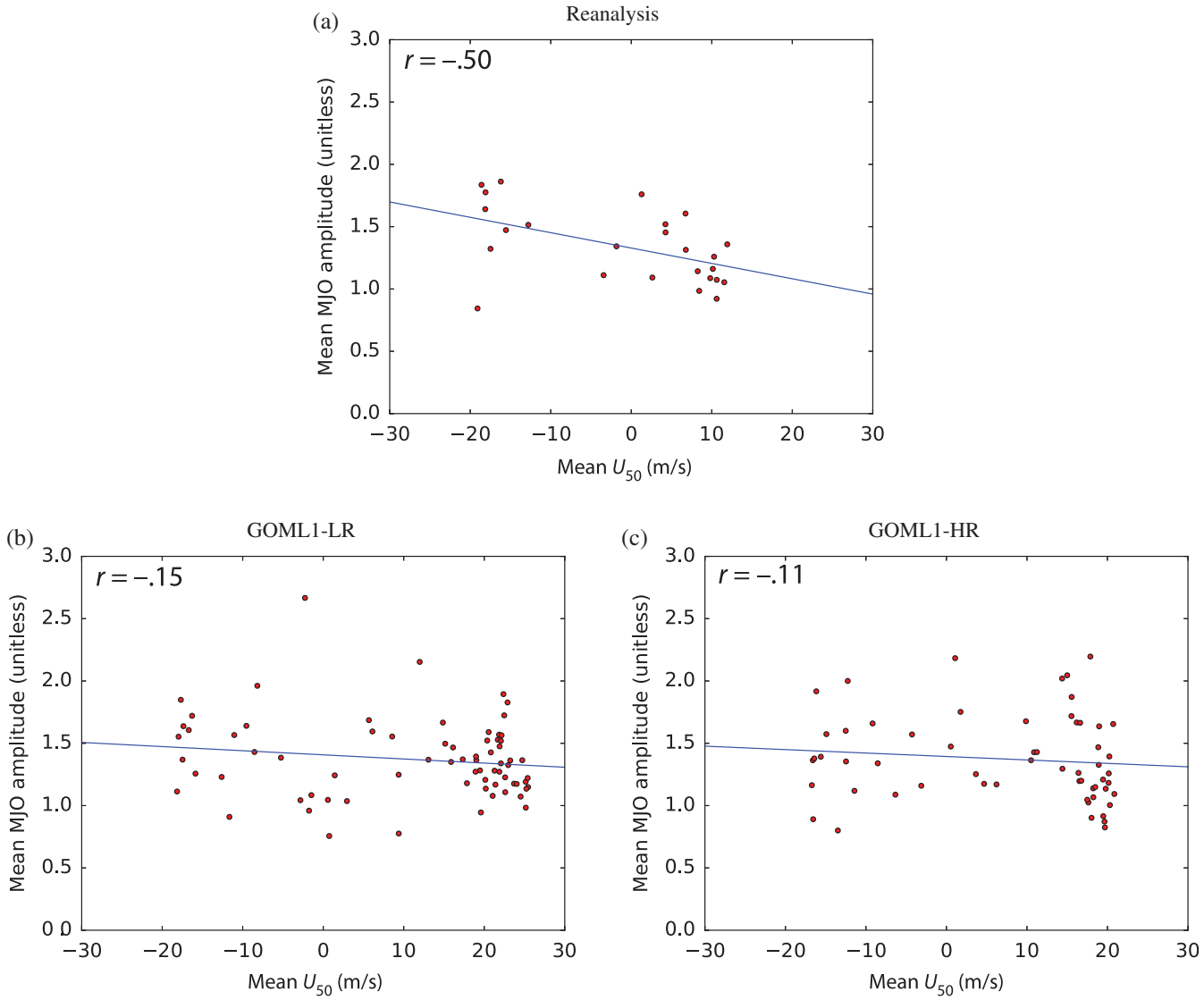

FIGURE 2 Relationship between DJF-mean MJO amplitude and U_{50} for (a) reanalysis, (b) GOML1-LR and (c) GOML1-HR. In (a), strong ENSO seasons are excluded. Number of samples is (a) 25, (b) 72 and (c) 58. The blue lines are least-squares regressions, with the Pearson's correlation coefficient (r) indicated at the top of the diagram

For GOML1, RMM indices are computed by projecting model data onto the Wheeler and Hendon (2004) empirical orthogonal functions, after first isolating sub-seasonal variability as in Wheeler and Hendon (2004). No ENSO filtering is performed as GOML1 never produces a Niño3.4 anomaly larger than ±1.0°C.

3 | RESULTS

3.1 | MJO and QBO in MetUM-GOML1

GOML1-LR and GOML1-HR capture well the observed spatial structure of QBO winds and MJO eastwards propagation (Figure 1) and compare favourably to most contemporary climate models (c.f., Charlton-Perez et al., 2012; Jiang et al., 2015). QBO winds are more meridionally confined in GOML1 than in ERA-Interim, particularly below 50 hPa, and extend to lower levels, closer to the tropopause. The QBO period, determined from Fourier analysis of $\overline{U}_{50}$, is 28 months in ERA-Interim, 33 months in GOML1-LR and 27 months in GOML1-HR (not shown). MJO propagation is composited on 100°E to focus on propagation across the Maritime Continent, where Son et al. (2017) found the strongest QBO-associated signal. GOML1-LR and GOML1-HR produce propagation that is slightly weaker than observed, but which has approximately the observed phase speed and period. Finer horizontal resolution does not substantially affect the simulated QBO or MJO in GOML1, as GOML1-LR and GOML1-HR are remarkably similar.

3.2 | Overall QBO–MJO relationship

Following Yoo and Son (2016), we compute correlations between DJF-mean MJO amplitude and $\overline{U}_{50}$ for reanalysis and GOML1 (Figure 2). As expected, reanalysis shows a statistically significant correlation at the 5% level when

excluding strong ENSO periods ($r = .50$) (Figure 2a). Excluding strong ENSO reduces any in-phase ENSO influence on the QBO–MJO relationship and provides a cleaner comparison to GOML1, which lacks ENSO.

Neither GOML1-LR nor GOML1-HR show a statistically significant QBO–MJO correlation ($r = -.15$ and $r = -.11$, respectively) (Figure 2b,c). This is surprising, given the strong connection in reanalysis and the robust simulation of the QBO and the MJO in GOML1. GOML1 produces a similar range of DJF-mean MJO amplitudes as observed, but displays excessive $\overline{U}_{50}$ variance. The WQBO is too strong: in many seasons the DJF-mean $\overline{U}_{50}$ exceeds 20 m/s, particularly in GOML1-LR. These strong WQBO conditions do not damp the MJO in GOML1, however. Strong and weak MJO amplitudes occur under WQBO and EQBO alike, producing considerable scatter about the least-squares regression lines in Figure 2b,c. Sub-sampling the GOML1 simulations to the same length as the ENSO-filtered reanalysis data set (25 DJFs) did not produce any statistically significant correlations at the 5% level (not shown); there are no 25-year periods in GOML1 when the QBO–MJO relationship is as strong as in reanalysis.

3.3 | QBO–MJO relationship by RMM phase

The lack of a QBO–MJO relationship in GOML1 could be due to compensating errors in the simulated effect of the QBO on the amplitude and frequency of individual RMM phases. To test this, we compute the frequency of active MJO days (RMM amplitude ≥ 1), as well as the mean RMM amplitude on active MJO days, for each RMM phase under EQBO and WQBO (Figure 3).

Reanalysis shows that EQBO favors stronger amplitudes over the Maritime Continent and West Pacific (phases 4–7) (Figure 3a), consistent with Yoo and Son (2016) and Son et al. (2017). This increased amplitude is associated with a reduced frequency of MJO active days, which may indicate an increased MJO phase speed (i.e., stronger events propagate more quickly) or fewer MJO events (Figure 3b). The latter may occur through a "discharge–recharge" mechanism (e.g., Benedict & Randall, 2007), whereby the "recharge" phase is longer after a stronger MJO event. WQBO is associated with weaker, but more frequent, MJO active days in the Indian Ocean and Maritime Continent. Near the Maritime Continent (phases 3–5), where the QBO–MJO relationship is strongest, changes in MJO frequency between EQBO and WQBO are anti-correlated with changes in MJO amplitude between EQBO and WQBO.

By contrast, GOML1-LR shows only slight amplitude increases in phases 4 and 5 during EQBO compared to WQBO, but much stronger amplitudes in the West Pacific and Western Hemisphere (phases 7 and 8) (Figure 3c). However, EQBO in GOML1-LR is associated with substantial increases in the frequency of MJO active days near the Maritime Continent; there are nearly twice as many active MJO days in phase 5 in EQBO as in WQBO (Figure 3d). MJO frequency decreases in the West Pacific in EQBO in GOML1-LR, compensating for the increases in amplitude. GOML1-HR also shows increased MJO amplitude in the West Pacific in EQBO relative to WQBO (phases 6 and 7) (Figure 3e), but strong reductions in amplitude for Indian Ocean and Maritime Continent phases (phases 2–4). Again, phases with reduced amplitude show increased frequency, while those with increased amplitude tend to show reduced frequency (Figure 3f). This suggests an opposite relationship between MJO amplitude and either phase speed or the number of events. In general, GOML1 fails to capture the observed increase in MJO amplitude over the Maritime Continent in EQBO, instead showing increased amplitudes over the West Pacific and increased MJO frequency over the Indian Ocean and Maritime Continent.

3.4 | QBO effects on tropical tropopause temperatures

Biases in the QBO–MJO relationship in GOML1 may be due to errors in simulated QBO-induced variations in temperatures and winds near the TTL, which Yoo and Son (2016) hypothesized as mechanisms for QBO modulation of MJO amplitude. Here, we focus on changes in TTL static stability by computing the difference in zonal-mean temperatures between EQBO and WQBO for ERA-Interim and MetUM-GOML1 (Figure 4). In ERA-Interim, EQBO is associated with a reduction in stability across the TTL, with cold temperature anomalies centered on the equator (Figure 4a), consistent with Nishimoto and Yoden (2017). We also compute departures from the zonal-mean temperatures, averaged 5°S–5°N. The difference between the EQBO and WQBO composites of these departures shows the longitudes at which the TTL anomalies in EQBO are relatively stronger or weaker. In ERA-Interim, the coldest TTL temperatures in EQBO are located at Indian Ocean and Maritime Continent longitudes (90°–150°E) (Figure 4b), consistent with the preference for stronger MJO amplitudes in those RMM phases (Figure 3a).

There are substantial biases in the simulated effect of the QBO on the TTL in GOML1 (Figure 4b–f). In GOML1-LR (Figure 4c) and GOML1-HR (Figure 4e), the QBO-related zonal-mean temperature anomalies are of the correct sign, but their magnitudes are far weaker than in ERA-Interim. The cooling near the TTL in EQBO displaced downwards, peaking near 100 hPa in GOML1 compared to 70 hPa in ERA-Interim, consistent with the displacement in the zonal-mean zonal wind (Figure 1). GOML1-HR produces stronger warming in EQBO at 30 hPa, reducing the bias, and improves the subtropical upper-tropospheric warming in each hemisphere, but shows weaker TTL cooling than GOML1-LR. These weak zonal-mean TTL temperature anomalies, and consequent weak anomalies in upper-tropospheric static stability, may be responsible for the lack

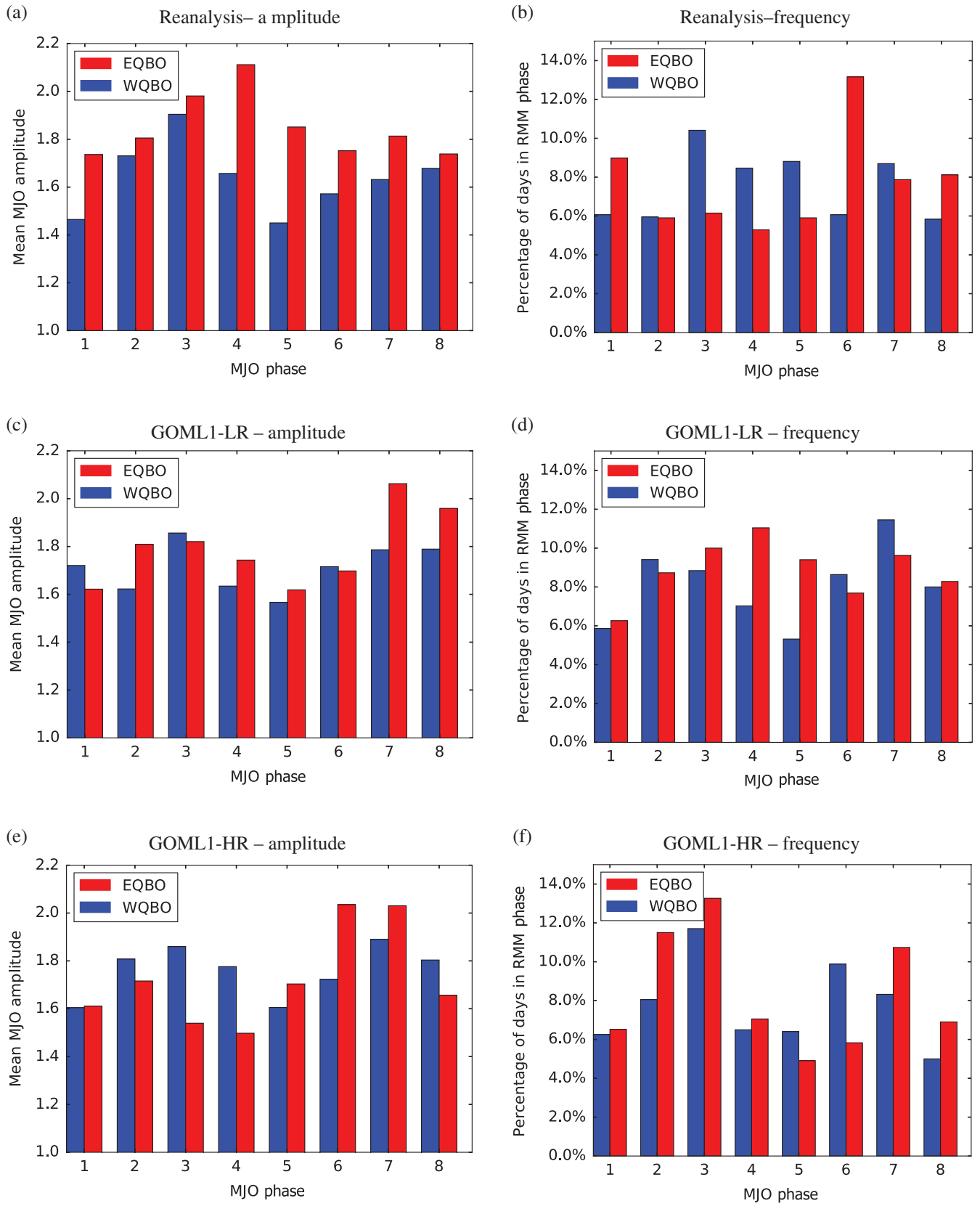

FIGURE 3 Panels (a), (c) and (e) show mean MJO amplitude by RMM phase and QBO phase, using only active MJO days in that phase; panels (b), (d) and (f) show frequency of strong MJO days by RMM phase and QBO phase, using (a, b) reanalysis, (c, d) GOML1-LR and (e, f) GOML1-HR

of a QBO–MJO relationship in GOML1. Considering departures from the zonal-mean temperature, the coldest TTL anomalies in EQBO in GOML1-LR and GOML1-HR occur over the eastern Maritime Continent and West Pacific longitudes (120°E–180°) (Figure 4d,f). This is consistent with the preference for stronger MJO amplitudes in the West

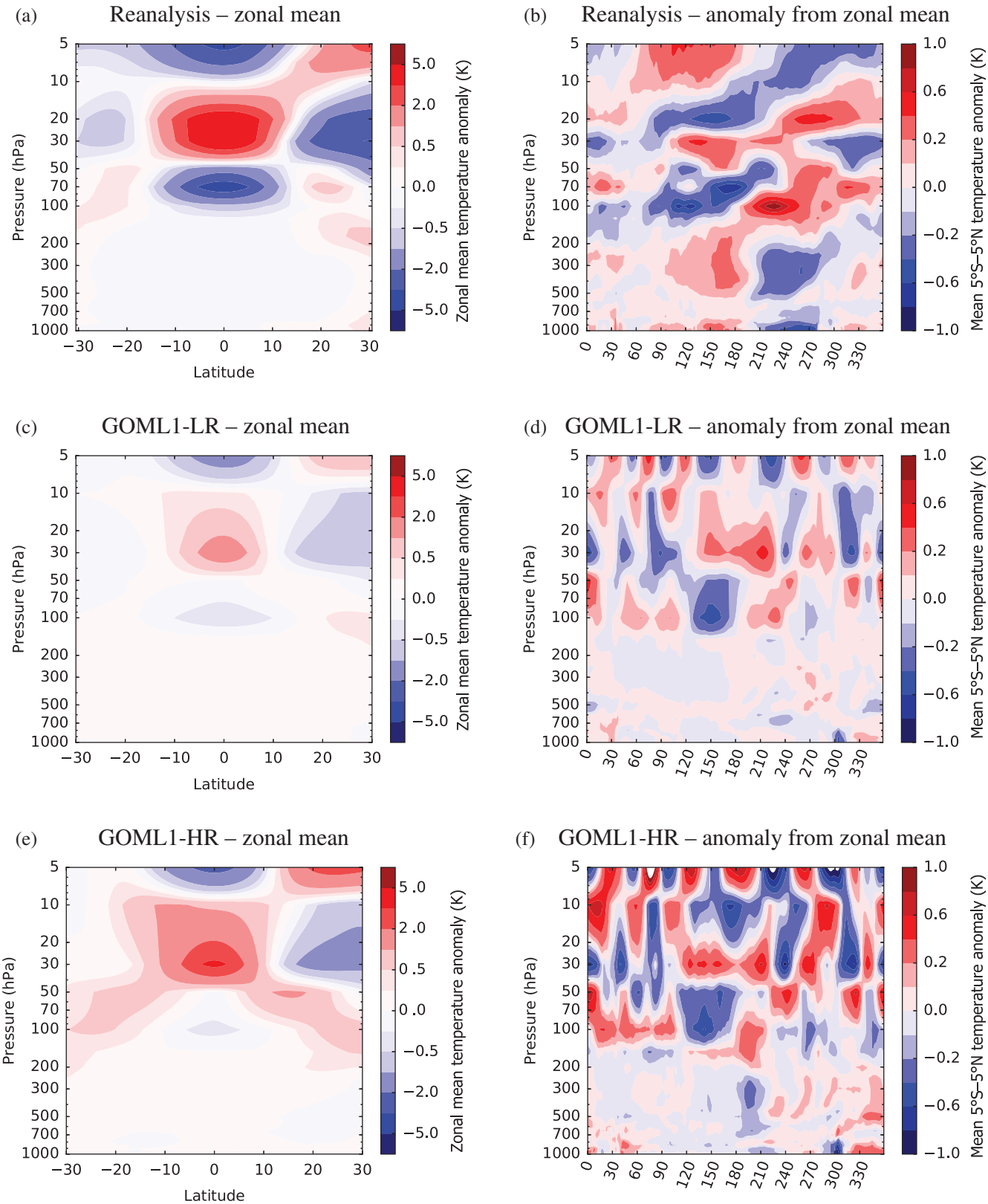

FIGURE 4 Panels (a), (c) and (e) show EQBO minus WQBO composites of DJF-mean, zonal-mean temperatures, averaged over all longitudes; panels (b), (d) and (f) show EQBO minus WQBO composites of departures from the zonal-mean temperatures, using data averaged 5°S–5°N. Data are from (a, b) ERA-Interim, (c, d) GOML1-LR and (e, f) GOML1-HR

Pacific in EQBO in GOML1 (Figure 3c,e). Combined with the ERA-Interim results above, this suggests that the zonal position of the coldest TTL temperature anomalies is linked to the phase of the strongest MJO activity.

4 | DISCUSSION AND CONCLUSIONS

We have investigated the QBO–MJO relationship in MetUM-GOML, a relatively simple coupled model

comprising a state-of-the-art atmospheric GCM coupled to a mixed-layer ocean. Our choice of MetUM-GOML was motivated by its ability to simulate the MJO, particularly in the configuration with increased convective mixing employed here (Klingaman & Woolnough, 2014a); MetUM coupled configurations with dynamic oceans struggle to represent the MJO in climate simulations (e.g., Jiang et al., 2015; Klingaman & Woolnough, 2014b). MetUM is also one of a small handful of "high-top" models capable of internally generating a QBO (e.g., Charlton-Perez et al., 2012).

GOML1 fails to capture the observed association between EQBO and stronger DJF MJO activity, in particular higher-amplitude MJO events near the Maritime Continent, despite a reasonable representation of the MJO and of the QBO winds. We postulate three hypotheses for this failure. First, the QBO-related temperature anomalies in GOML1 may be too weak to influence MJO convection, or biases in the spatial structure of the anomalies may suppress their effect (Figure 4). GOML1 produces an EQBO cold TTL temperature anomaly that is less than 25% of the magnitude of those in ERA-Interim; the maximum anomalies are shifted lower in the upper-troposphere (from 70 to 100 hPa) and eastwards from the Maritime Continent to the West Pacific relative to ERA-Interim. This hypothesis could be tested in further GOML simulations by nudging the stratospheric temperatures. If verified, this hypothesis would lend support to changes in static stability as the primarily mechanism for the QBO to influence the MJO.

Second, the GOML1 MJO may not be sufficiently sensitive to the QBO-induced changes in the upper-tropospheric mean state. GCM representations of the MJO suffer from biases in the vertical structure of convection and associated circulations (e.g., Klingaman et al., 2015), which may influence their response to QBO-associated TTL temperature and wind anomalies. Our GOML1 configuration used higher entrainment and detrainment rates to improve the MJO, but increasing these rates is known to suppress the depth of convection (Klingaman & Woolnough, 2014a), such that convection may terminate before it can "access" QBO-induced static stability anomalies at the TTL.

Finally, the observed QBO–MJO relationship may be an artifact of a limited sample size—there are only 25 DJFs in the ENSO-filtered data set—or of a nonlinear (e.g., Butler, Polvani, & Deser, 2014) or lagged effect of ENSO. Son et al. (2017) found a negligible in-phase ENSO–MJO relationship in boreal winter over the Maritime Continent, but a strong QBO–MJO relationship. However, strong El Niño events may influence the QBO for 2–4 years after the El Niño decays (Christiansen, Yang, & Madsen, 2016), an effect that would not be removed by filtering out only strong ENSO seasons as in Yoo and Son (2016). ENSO may also alter the QBO period by influencing the speed of the downwards propagation of QBO winds (Yuan, Geller, & Love, 2014). If an ENSO effect lingers in the reanalysis QBO–MJO relationship, then GOML1 cannot be expected to reproduce it, as the model lacks an ENSO.

Using multi-decadal MetUM-GOML1 simulations at two resolutions (≈200 and ≈90 km at the equator), we have shown that the model cannot reproduce the observed association between the Northern Hemisphere winter QBO and MJO activity around the Maritime Continent, whether measured by overall MJO amplitude or the amplitude of individual MJO phases. Where observations show increased amplitude and reduced MJO frequency near the Maritime Continent in EQBO phases, MetUM-GOML1 displays little change to amplitude and increased MJO frequency. Instead, EQBO in MetUM-GOML1 is associated with increased MJO amplitude in the West Pacific, which may be due to the model's tendency to place the QBO-associated TTL static stability anomalies in that sector, rather than over the Maritime Continent as in ERA-Interim. These increases in MJO amplitude in West Pacific are compensated by reductions in amplitude in other phases, however, to give no QBO effect on overall amplitude. The failure of MetUM-GOML1 to simulate the observed QBO–MJO relationship may be due to a combination of errors in QBO vertical and horizontal structure, weak QBO-induced TTL temperature anomalies, biases in the vertical structure of MJO convection, or the observed relationship being an artifact of either a limited sample size or nonlinear or lagged ENSO effects on the QBO. It is clear that successful simulation of the QBO and MJO is a necessary, but not sufficient, condition to capture their teleconnection.

ACKNOWLEDGEMENTS

N.P.K. was supported by an Independent Research Fellowship from the UK Natural Environment Research Council (NE/L010976/1). The authors are grateful for discussions with Steve Woolnough and Andrew Charlton-Perez. The authors are grateful for the suggestions of two reviewers, which helped to improve the clarity and presentation of the manuscript. MetUM-GOML1 simulations were performed on ARCHER, the UK national supercomputing service. MetUM-GOML1 data are available on request from the corresponding author, through the JASMIN Collaborative Analysis Platform (http://www.jasmin.ac.uk; Lawrence et al., 2013). RMM indices can be downloaded from the Australian Bureau of Meteorology: http://www.bom.gov.au/climate/mjo/graphics/rmm.74toRealtime.txt. ERA-Interim data are available from ECMWF: https://www.ecmwf.int/en/research/climate-reanalysis/era-interim. Hadley Centre SST data can be obtained from the Met Office: https://www.metoffice.gov.uk/hadobs/hadisst/.

Conflict of interests

The authors declare no potential conflict of interests.

Author contributions

J.C.K.L. (lead author) analysed reanalysis data and model simulations; N.P.K. (contributing author) performed model simulations.

ORCID

Nicholas P. Klingaman http://orcid.org/0000-0002-2927-9303

REFERENCES

Baldwin, M., Gray, L., Dunkerton, T., Hamilton, K., Haynes, P., Randel, W., … Takahashi, M. (2001). The quasi-biennial oscillation. *Reviews of Geophysics*, *39*, 179–229.

Benedict, J. J., & Randall, D. A. (2007). Observed characteristics of the MJO relative to maximum rainfall. *Journal of the Atmospheric Sciences*, *64*, 2332–2354.

Bush, S. J., Turner, A. G., Woolnough, S. J., Martin, G. M., & Klingaman, N. P. (2015). The effect of increased convective entrainment on Asian monsoon biases in the MetUM General Circulation Model. *Quarterly Journal of the Royal Meteorlogical Society*, *141*, 311–326.

Butler, A. H., Polvani, L. M., & Deser, C. (2014). Separating the stratospheric and tropospheric pathways of the El Niño–Southern Oscillation. *Environmental Research Letters*, *9*, 024014.

Charlton-Perez, A. J., Baldwin, M. P., Birner, T., Black, R. X., Butler, A. H., Calvo, N., … Watanabe, S. (2012). On the lack of stratospheric dynamical variability in low-top versions of the CMIP5 models. *Journal of Geophysical Research*, *118*, 2494–2505.

Christiansen, B., Yang, S., & Madsen, M. S. (2016). Do strong warm ENSO events control the phase of the stratospheric QBO? *Geophysical Research Letters*, *43*, 10489–10495.

Collimore, C. C., Martin, D. W., Hitchman, M. H., Huesmann, A., & Waliser, D. E. (2003). On the relationship between the QBO and tropical deep convection. *Journal of Climate*, *16*, 2552–2568.

Dee, D., Uppala, S., Simmons, A., Berrisford, P., Poli, P., Kobayashi, S., … Vitart, F. (2011). The ERA-Interim reanalysis: Configuration and performance of the data assimilation system. *Quarterly Journal of the Royal Meteorological Society*, *137*, 553–597.

Fueglistaler, S., Dessler, A., Dunkerton, T., Folkins, I., Fu, Q., & Mote, P. W. (2009). Tropical tropopause layer. *Reviews of Geophysics*, *47*, RG1004.

Garfinkel, C. I., & Hartmann, D. L. (2011). The influence of the quasi-biennial oscillation on the troposphere in winter in a hierarchy of models. Part I: Simplified dry GCMs. *Journal of the Atmospheric Sciences*, *68*, 1273–1289.

Giorgetta, M. A., Bengtsson, L., & Arpe, K. (1999). An investigation of QBO signals in the East Asian and Indian monsoon in GCM experiments. *Climate Dynamics*, *15*, 435–450.

Hardiman, S. C., Butchart, N., Hinton, T. J., Osprey, S. M., & Gray, L. J. (2012). The effect of a well-resolved stratosphere on surface climate: Differences between CMIP5 simulations with high and low top versions of the Met Office climate model. *Journal of Climate*, *25*, 7083–7099.

Hirons, L. C., Klingaman, N. P., & Woolnough, S. J. (2015). MetUM-GOML: A near-globally coupled atmosphere–ocean mixed-layer model. *Geoscientific Model Development*, *8*, 363–379.

Huang, B., Hu, Z.-Z., Kinter, J. L., Wu, Z., & Kumar, A. (2012). Connection of stratospheric QBO with global atmospheric general circulation and tropical SST. Part I: Methodology and composite life cycle. *Climate Dynamics*, *38*, 1–23.

Hudson, D., Marshall, A. G., Yin, Y., Alves, O., & Hendon, H. H. (2013). Improving intraseasonal prediction with a new ensemble generation strategy. *Monthly Weather Reviews*, *141*, 4429–4449.

Hurrell, J. W., Hack, J. J., Shea, D., Caron, J. M., & Rosinski, J. (2008). A new sea surface temperature and sea ice boundary data set for the community atmospheric model. *Journal of Climate*, *21*, 5145–5153.

Jiang, X., Waliser, D. E., Xavier, P. K., Petch, J., Klingaman, N. P., Woolnough, S. J., … Zhu, H. (2015). Vertical structure and physical processes of the Madden–Julian oscillation: Exploring key model physics in climate simulations. *Journal of Geophysical Research*, *120*, 4718–4748.

Kang, I.-S., Jang, P.-H., & Almazroui, M. (2014). Examination of multi-perturbation methods for ensemble prediction of the MJO during boreal summer. *Climate Dynamics*, *42*, 2627–2637.

Klingaman, N., & Woolnough, S. (2014a). Using a case-study approach to improve the Madden–Julian oscillation in the Hadley Centre model. *Quarterly Journal of the Royal Meteorological Society*, *140*, 2491–2505.

Klingaman, N. P., Jiang, X., Xavier, P. K., Petch, J., Waliser, D., & Woolnough, S. J. (2015). Vertical structure and physical processes of the Madden–Julian oscillation: Synthesis and summary. *Journal of Geophysical Research*, *120*, 4671–4689.

Klingaman, N. P., & Woolnough, S. J. (2014b). The role of air–sea coupling in the simulation of the Madden–Julian oscillation in the Hadley Centre model. *Quarterly Journal of the Roayl Meteorological Society*, *140*, 2272–2286.

Lawrence, B. N., Bennett, V. L., Churchill, J., Juckes, M., Kershaw, S. P., Pepler, S., … Stephens, A. (2013). Storing and manipulating environmental big data with JASMIN. In *2013 IEEE international conference on big data* (pp. 68–75). San Francisco, CA: IEEE.

Liu, P., Zhang, Q., Zhang, C., Zhu, Y., Khairoutdinov, M., Kim, H.-M., … Zhang, M. (2016). A revised real-time multivariate MJO index. *Monthly Weather Reviews*, *144*, 627–642.

Madden, R. A., & Julian, P. R. (1971). Detection of a 40–50 day oscillation in the zonal wind in the tropical Pacific. *Journal of the Atmospheric Sciences*, *28*, 702–708.

Marshall, A. G., Hendon, H. H., Son, S.-W., & Lim, Y. (2017). Impact of the quasi-biennial oscillation on predictability of the Madden–Julian oscillation. *Climate Dynamical*, *49*, 1365–1377.

Nie, J., & Sobel, A. H. (2015). Responses of tropical deep convection to the QBO: Cloud-resolving simulations. *Journal of the Atmospheric Sciences*, *72*, 3625–3638.

Nishimoto, E., & Yoden, S. (2017). Influence of the stratospheric quasi-biennial oscillation on the Madden–Julian oscillation during austral summer. *Journal of the Atmospheric Sciences*, *74*, 1105–1125.

Osprey, S. M., Grey, L. J., Hardiman, S. C., Butchart, N., & Hinton, T. J. (2013). Stratospheric variability in twentieth-century CMIP5 simulations of the Met Office climate model: High top versus low top. *Journal of Climate*, *26*, 1595–1606.

Rayner, N., Parker, D. E., Horton, E., Folland, C., Alexander, L., Rowell, D., … Kaplan, A. (2003). Global analyses of sea surface temperature, sea ice, and night marine air temperature since the late nineteenth century. *Journal of Geophysical Research*, *108*, 4407.

Shelly, A., Xavier, P., Copsey, D., Johns, T., Rodríguez, J. M., Milton, S., & Klingaman, N. (2014). Coupled versus uncoupled hindcast simulations of the Madden–Julian oscillation in the year of tropical convection. *Geophysical Research Letters*, *41*, 5670–5677.

Smith, D. M., & Murphey, J. M. (2007). An objective ocean temperature and salinity analysis using covariances from global climate models. *Journal of Geophysical Research*, *112*, C02022.

Son, S.-W., Lim, Y., Yoo, C., Hendon, H., & Kim, J. (2017). Stratospheric control of Madden–Julian oscillation and its teleconnection. *Journal of Climate*, *30*, 1909–1922.

Walters, D. N., Best, M. J., Bushell, A. C., Copsey, D., Edwards, J. M., Falloon, P. D., … Williams, K. D. (2011). The Met Office Unified Model Global Atmosphere 3.0/3.1 and JULES Global Land 3.0/3.1 configurations. *Geoscientific Model Development*, *4*, 919–941.

Wheeler, M. C., & Hendon, H. H. (2004). An all-season real-time multivariate MJO index: Development of an index for monitoring and prediction. *Monthly Weather Reviews*, *132*, 1917–1932.

Wu, J., Ren, H.-L., Zuo, J., Zhao, C., Chen, L., & Li, Q. (2016). MJO prediction skill, predictability, and teleconnection impacts in the Beijing Climate Center Atmospheric General Circulation Model. *Dynamics of Atmospheres and Oceans*, *75*, 78–90.

Yoden, S., Bui, H.-H., & Nishimoto, E. (2014). A minimal model of QBO-like oscillation in a stratosphere–troposphere coupled system under a radiative-moist convective quasi-equilibrium state. *SOLA*, *10*, 112–116.

Yoo, C., & Son, S.-W. (2016). Modulation of the boreal wintertime Madden–Julian oscillation by the stratospheric quasi-biennial oscillation. *Geophysical Research Letters*, *43*, 1392–1398.

Yuan, W., Geller, M. A., & Love, P. T. (2014). ENSO influence on QBO modulations of the tropical tropopause. *Quarterly Journal of the Royal Meteorological Society*, *140*, 1670–1676.

Zhang, C. (2005). Madden–Julian oscillation. *Reviews of Geophysics*, *43*, RG2003.

How to cite this article: Lee JCK, Klingaman NP. The effect of the quasi-biennial oscillation on the Madden–Julian oscillation in the Met Office Unified Model Global Ocean Mixed Layer configuration. *Atmos Sci Lett*. 2018;1–9. https://doi.org/10.1002/asl.816